

A Dual Cobalt-Photoredox Catalytic Approach for Asymmetric Dearomatization of Indoles with Aryl Amides via C–H Activation

Abir Das, Subramani Kumaran, Harihara Subramanian Ravi Sankar, J. Richard Premkumar, and Basker Sundararaju*

Abstract: In this study, we unveil a novel method for the asymmetric dearomatization of indoles under cobalt/photoredox catalysis. By strategically activating C–H bonds of amides and subsequent migratory insertion of π -bonds present in indole as reactive partner, we achieve *syn*-selective tetrahydro-5*H*-indolo[2,3-*c*]isoquinolin-5-one derivatives with excellent yields and enantiomeric excesses of up to >99%. The developed method operates without a metal oxidant, relying solely on oxygen as the oxidant and employing an organic dye as a photocatalyst under irradiation. Control experiments and stoichiometric studies elucidate the reversible nature of the enantiodetermining C–H activation step, albeit not being rate-determining. This study not only expands the horizon of cobalt-catalyzed asymmetric C–H bond functionalization, but also showcases the potential synergy between cobalt and photoredox catalysis in enabling asymmetric synthesis of complex molecules.

Introduction

Faraday's serendipitous discovery of benzene unveiled the doorway to a realm of molecules that would shape the course of modern chemistry.^[1] Over the past decade, the annual production of aromatic scaffolds has reached up to 100 million tons. Therefore, there has been a concerted effort to harness the abundant reservoir of flat aromatic molecules and elevate them into value-added, three-dimensional, complex molecular architectures.^[2–5] However, due to unparallel stability^[6–8] offered by the aromatic compounds through delocalization of π -electrons within their molecular framework empowers them to engage in a myriad of chemical transformations while preserving their aromatic character.^[9–10] Alternatively, uncovering strat-

egies to disrupt aromaticity presents a promising avenue for generating novel molecular frameworks from widely available aromatic hydrocarbons.^[11–12] Besides traditional approaches,^[13–17] hydrogenation,^[18] nucleophilic addition^[19] mediated by transition metals, and selective 1,2-hydroxylation mediated by enzymes^[20] are among the known examples in the literature. In recent years, catalytic asymmetric dearomatization reactions have gained prominence as a potent synthetic methodology to access complex molecular architectures.^[2–3,5] This approach facilitates the transformation of various π -bonds present in the aromatic compounds as a reactive functional group, thereby enabling their utilization in creation of chiral molecules. Among the aromatic scaffolds, phenol and its derivatives,^[11,21–23] indole,^[12] and other heteroarenes^[24] have been extensively used in asymmetric dearomatization via cyclo addition,^[19] allylic substitution,^[25] hydrogenation,^[18] arenophile-mediated dearomatization,^[26] etc. However, Activation of inert C–H bond and subsequent coupling of π -bonds that involved in aromaticity is seldom explored.^[27–29] In this regard, You and co-workers reported the novel chiral Cp^*Rh -catalyzed asymmetric dearomatization of 2-naphthols with alkyne via ortho-C–H bond activation of the 1-phenyl-2-naphthol derivatives.^[27] Xu and Lu recently reported the cascade intramolecular C–C and C–H activation strategy catalyzed by $\text{Rh(I)/(S)}\text{-dtbm-Segphos}$ to access complex tetra cyclic core.^[28]

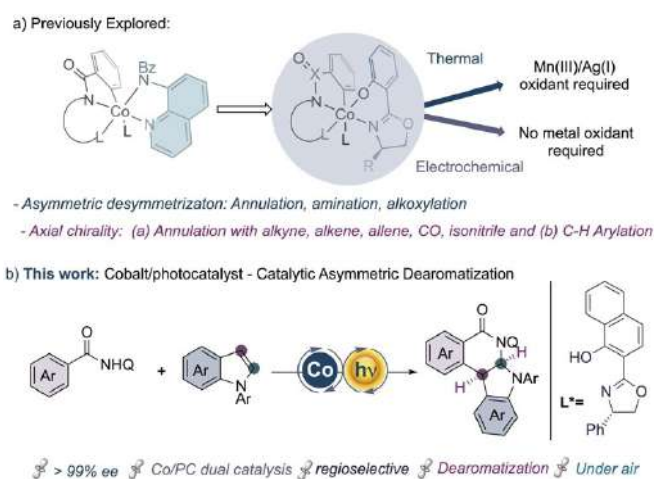
On the other hand, The field of cobalt-catalyzed C–H bond functionalization has witnessed remarkable expansion since the seminal work by Daugulis,^[30] particularly in the realm of bidentate-directing group-assisted transformations.^[31] Recent developments have witnessed a shift towards sustainable methodologies, with investigations into the replacement of traditional oxidants like Mn(III) or Ag(I) with photocatalysts under irradiation^[32b–d] or utilizing electricity as the sole oxidant.^[32a–b]

Additionally, a profound understanding of the active octahedral cobaltacycles^[33] formed in situ has led to breakthroughs in asymmetric catalysis facilitated by the use of simple cobalt(II) salts and enantiopure Salox ligands as chiral sources.^[34–35] This novel strategy has been explored led by Shi, Ackermann and Niu in cobalt-catalyzed asymmetric C–H bond functionalizations encompassing diverse transformations such as annulation with alkynes, alkenes, allenes, isonitriles as well as C–H arylation, under both thermal and electrochemical

[*] A. Das, Dr. S. Kumaran, H. S. Ravi Sankar, Prof. Dr. B. Sundararaju
 Department of chemistry,
 Indian Institution of Technology Kanpur,
 Kanpur, Uttar Pradesh, India—208 016
 E-mail: basker@iitk.ac.in
 J. R. Premkumar
 PG & Research Department of Chemistry,
 Bishop Heber College,
 Tiruchirappalli-620017, Tamil Nadu, India

conditions.^[36] Furthermore, the topic has been explored for asymmetric desymmetrization of phosphinamides through C–C, C–O and C–N bond formation with alkynes, alcohols, amines under mild conditions (Scheme 1a).^[37]

To the best of our knowledge, the asymmetric dearomatization of indoles coupled with C–H activation catalyzed by cobalt remains unexplored. Furthermore, utilization of a photocatalyst under irradiation to supplant the stoichiometric quantities of Mn(III) or Ag(I) in cobalt(II)-catalyzed asymmetric C–H bond functionalizations has not been documented. However, it is noteworthy that electricity has been successfully employed as a sole oxidant in these contexts for asymmetric C–H bond functionalization with cobalt, circumventing the need for Mn(III) and Ag(I).^[36b,e,h,37c–e] Previously, our research effort have achieved notable advancements in C–H bond annulation and alkynylation by synergistically employing cobalt and photocatalyst under oxidant-free conditions, resulting in racemic products.^[32d] Notably, these efforts have yielded successful outcomes with alkyne, alkene, and bromoalkyne substrates.^[38,39] However, the transition to an asymmetric variant using the cobalt/PS dual catalytic approach has remained a formidable challenge. This challenge arises due to the lack of systematic validation of chiral ligands and the intricate interplay between the photocatalyst and the enantio-determining step. In this study, we unveil the novel method for the asymmetric dearomatization of indole. This process involves the enantio-determining C–H bond activation of amides, followed by the migratory insertion of the π -bond of the indole, essential for preserving aromaticity under cobalt/photoredox catalysis. This strategic approach results in the synthesis of *syn*-selective tetrahydro-5*H*-indolo[2,3-*c*]isoquinolin-5-one derivatives in excellent yields, with enantiomeric excess reaching up to > 99 % (Scheme 1b).



Scheme 1. Overview of Ligand enabled Co(III) catalysis and asymmetric C–H bond functionalizations.

Results and Discussion

In our pursuit of achieving enantioselective dearomatization of indoles through C–H and N–H bond annulation strategies, we initiated our preliminary investigation employing *N*-(quinolin-8-yl)benzamide **1a** as the limiting reagent and 1-(pyrimidin-2-yl)-1*H*-indole **2a** as the coupling partner. Under the catalytic system comprising 20 mol % Co(OAc)₂·4H₂O, 30 mol % (*S*)-Salox ((*S*)-**L1**) as the chiral ligand, 10 mol % Na₂EosinY as the photocatalyst, and 2.0 equiv. NaOPiv as the additive in 2,2,2-trifluoroethanol (TFE), and irradiation with white LED bulbs (7 W×4) for 36 h, the dearomatized product **3aa** was obtained in 45 % yield with 79 % ee as a single regioisomer (entry 1, Table 1). The structure of **3aa** was confirmed through X-ray crystallographic analysis, and its absolute stereochemistry was assigned as (*R,R*)-configuration.^[40]

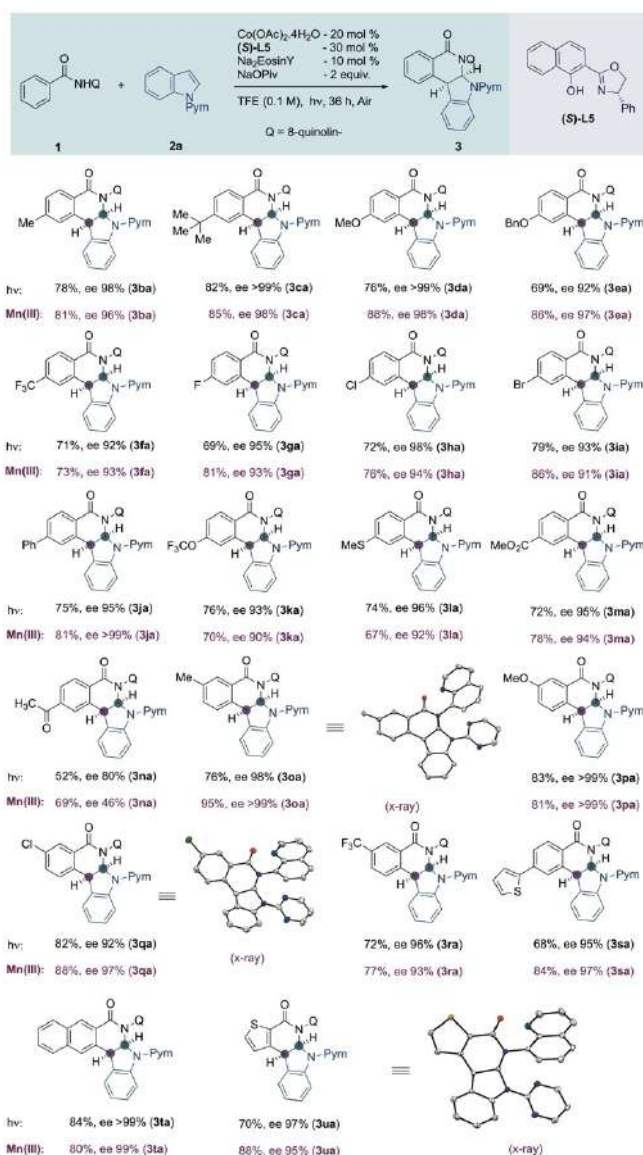
Table 1: Reaction optimization^[a]

Entry	L	Base	Solvent	Yield (%) ^[b]	ee (%) ^[c]
1	(<i>S</i>)- L1	NaOPiv	TFE	45	79
2	(<i>S</i>)- L1	NaOPiv	EtOH	n.d.	n.d.
3	(<i>S</i>)- L1	NaOPiv	HFIP	25	59
4	(<i>S</i>)- L1	NaOPiv	^t BuOH	n.r.	n.d.
5	(<i>S</i>)- L2	NaOPiv	TFE	55	24
6	(<i>S</i>)- L3	NaOPiv	TFE	33	92
7	(<i>S</i>)- L4	NaOPiv	TFE	n.d.	n.d.
8	(<i>S</i>)- L5	NaOPiv	TFE	85	95
9	(<i>S</i>)- L5	PivOH	TFE	22	48
10	–	NaOPiv	TFE	n.r.	n.d.
11	(<i>S</i>)- L5	–	TFE	n.r.	n.d.
12	(<i>S</i>)- L5	NaOPiv	TFE	n.r.	n.d. ^[d]
13	(<i>S</i>)- L5	NaOPiv	TFE	n.r.	n.d. ^[e]
14	(<i>S</i>)- L5	NaOPiv	TFE	n.r.	n.d. ^[f]
15	(<i>S</i>)- L5	NaOPiv	TFE	n.r.	n.d. ^[g]
16	(<i>S</i>)- L5	NaOPiv	TFE	89	98 ^[h]
17	(<i>S</i>)- L5	NaOPiv	TFE	71	91 ^[i]
18	(<i>R</i>)- L5	NaOPiv	TFE	61	95 ^[j]

[a] All reactions were carried out under air unless otherwise stated using **1a** (0.1 mmol), **2a** (0.15 mmol), Co(OAc)₂·4H₂O (20 mol %), Na₂EosinY (10 mol %), Salox **L** (30 mol %), and NaOPiv (0.20 mmol) in TFE (1.0 mL) under irradiation for 36 h. [b] Isolated yield. [c] The *ee* values were determined by chiral HPLC analysis. [d] without Co(OAc)₂·4H₂O [e] without Na₂EosinY [f] Performed under argon. [g] Performed under dark. [h] Performed with Mn(OAc)₂·4H₂O (0.1 mmol) at room temperature without any photocatalyst or under irradiation. [i] Performed in 1.0 mmol scale. [j] (*S,S*)-**3aa** was obtained with (*R*)-**L5**. TFE=2,2,2-Trifluoroethanol, n.r.=no reaction, n.d.=not determined.

To optimize the reaction conditions, we conducted systematic screenings of various solvents and chiral Salox ligands (entries 2–8). Among the solvents tested, TFE was found to be optimal, yielding the expected product **3aa** with moderate yields and good *ee* (entries 1–4). Considering the significant role of the Salox ligand in the reaction, we explored different ligand modifications to enhance both yield and enantiomeric excess (entries 5–8). Through quick screening of stereo-electronically biased Salox ligands (*S*)-**L2**–(*S*)-**L5**, (*S*)-**L5** emerged as the most promising ligand, affording an *ee* of up to 95 % and a yield of 85 % (entry 8). Further fine-tuning of sodium pivalate to pivalic acid did not improve the yield or *ee*, suggesting that cobaltacycle formation is assisted by the carboxylate base (entry 9). Control experiments were conducted to elucidate the role of each parameter in the dearomatization protocol (entries 10–15). The absence of cobalt salt, Salox ligand, or base hindered the reaction, indicating their essential role in the activation and functionalization of the C–H bond (entries 10–12). Furthermore, without Na₂EosinY, no product formation was observed, highlighting the crucial role of the photocatalyst in oxidizing the cobalt (entry 13). An experiment conducted under argon or in the dark condition demonstrated the necessity of irradiation for product formation and the role of air/oxygen (entries 14–15). To compare the results, the similar reaction was setup with Mn(III) (generated in situ from Mn(II) in the presence of oxygen from air) as oxidant at room temperature under standard conditions resulted in 89 % isolated yield of **3aa** (*R,R*) with 98 % *ee* (entry 16). To validate the practicality of the developed protocol, a 1.0 mmol scale reaction was performed, yielding the dearomatized product **3aa** with 71 % yield and 91 % *ee* (entry 17). Additionally, we tested other bidentate directing groups such as pyridine, benzoxazole, and aza-indole, but found them unsuitable under the reaction conditions (see the Supporting Information).^[41] Employing (*R*)-**L5** ligand instead of the (*S*)-variant resulted in the formation of the opposite isomer of **3aa**, i.e. (*S,S*)-**3aa**, in 61 % yield with 95 % *ee* (entry 18).^[40]

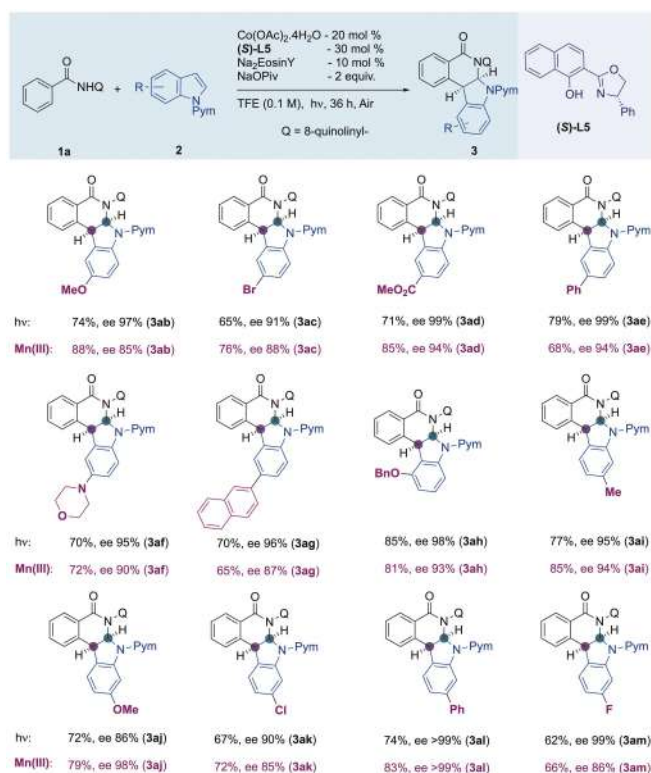
Upon employing optimized conditions, we initiated an exploration into the scope of benzamides, as delineated in Scheme 2. A diverse range of benzamides, featuring both *para*- and *meta*-substitutions, exhibited broad functional group tolerance and afforded the dearomatized annulated products in good-to-excellent yields and excellent enantioinduction. Substitutions encompassing various electron-donating (Me–, –*i*Bu, –MeO, –OBn) and electron-withdrawing (–CF₃, –F, –Cl, –Br, –Ph, –OCF₃, –SMe, –CO₂Me, –COMe) groups (**1b**–**1n**) at the *para*-position demonstrated suitability for the dearomatization process, yielding products within the range of 52 % to 82 %, and enantiomeric excess (*ee*) values spanning from 92 % to >99 %. In the case of meta-substituted benzamides, annulation favoured at the less hindered site, furnishing products (**3oa**–**3ra**) with yields ranging from 72 % to 83 % and *ee* values spanning from 92 % to >99 %. More interestingly, aromatic arene containing strong coordinating group such as sulphur group in 2-thienyl at the *para*-



Scheme 2. Scope of aryl amides. The products obtained at room temperature (28–30 °C) using **1** (0.1 mmol), **2a** (0.15 mmol), Co(OAc)₂·4H₂O (20 mol %), Salox **L** (30 mol %), Mn(OAc)₂·4H₂O (0.1 mmol) and NaOPiv (0.20 mmol) in TFE (1.0 mL) for 36 h.

position is tolerable and provide the expected product **3sa** in good yield and 95 % *ee*. Even naphthyl, thiophene based amides were also amenable and provide the annulated compound in 84 % and 70 % yield with >99 % and 97 % *ee* respectively. Validation of the stereochemistry and structural elucidation of **3qa**, **3oa**, and **3ua** was achieved through X-ray crystallography.^[40]

We next examined the suitability of various stereo-electronically biased *N*-pyrimidyl indole derivatives under optimized reaction conditions (Scheme 3). A broad spectrum of electron-donating and electron-withdrawing functional groups, such as –OMe, –Me, –NR₂, and –CO₂Me, –Br, –Ar positioned at the C-4, C-5 and C-6 sites of indole, exhibited excellent tolerance, affording the desired products (**3ab**–**3am**) in moderate-to-good yields (62–

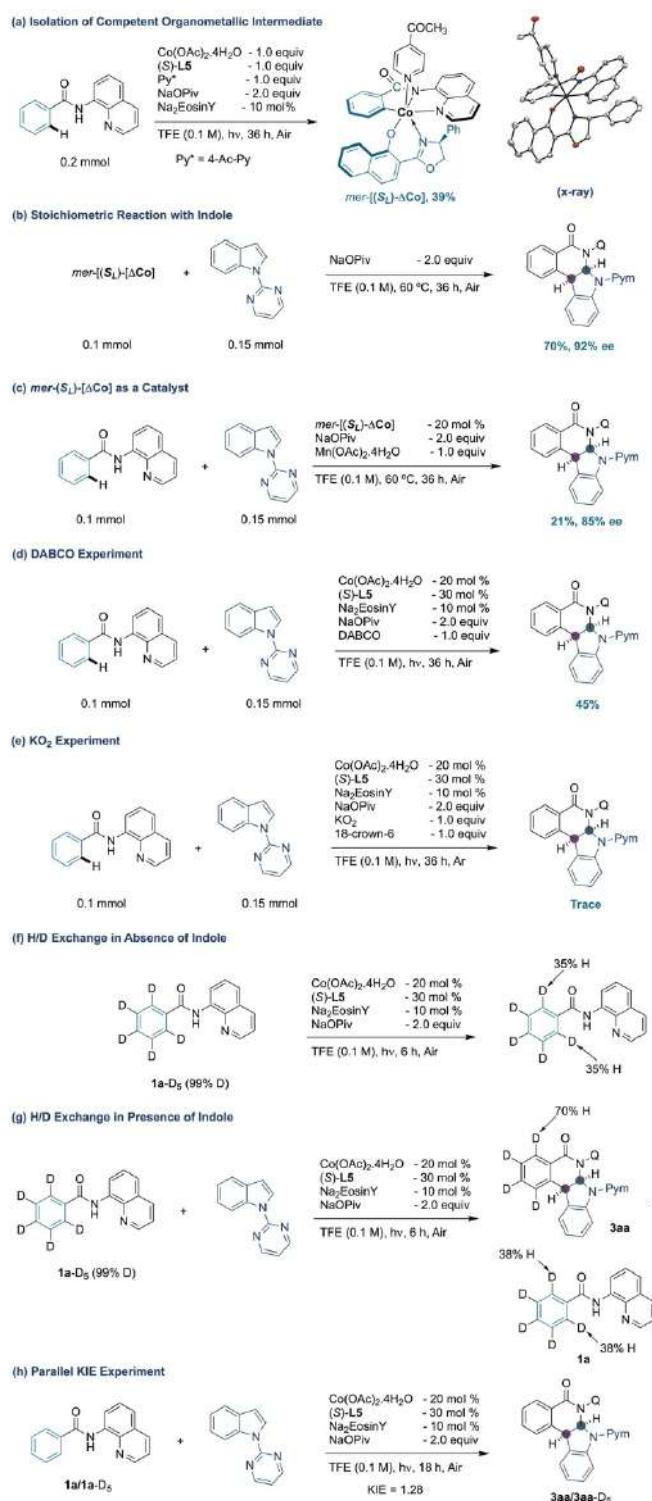


Scheme 3. Scope of Indole. The products obtained from at room temperature (28–30 °C) using **1** (0.1 mmol), **2a** (0.15 mmol), Co(OAc)₂·4H₂O (20 mol %), (S)-L5 (30 mol %), Na₂EosinY (10 mol %), NaOPiv (0.2 mmol) in TFE (1.0 mL) for 36 h.

85 %) with enantioinduction ranging from 86 to > 99 %. Notably, reactions involving substrates bearing sensitive and synthetically useful functional groups such as –F (**2m**), –Cl (**2k**), –Br (**2c**), and –OBn (**2h**) proceeded smoothly, and the resultant products were available for further derivatizations.

Indoles featuring sterically hindered phenyl (**2e**, **2i**) and naphthyl (**2g**) moieties were also found to be compatible, providing the target products in good yields (62–79 % yield, 92–> 99 % ee, respectively). Furthermore, to validate the protocol's applicability, biologically relevant indole **1f** was subjected to the optimized conditions, yielding the desired product **3af** in good yield (70 %) and with high enantiopurity (95 % ee). The scope of aryl amides and indole were also performed using Mn(III) as oxidant at room temperature (without Photocatalyst and no irradiation), and their results were given in Scheme 2 and 3 for comparison.

Following the scope of our experimental work, we conducted a series of control experiments and Density Functional Theory (DFT) calculations aimed at elucidating the mechanistic underpinnings of the asymmetric dearomative coupling of indole with aryl amides, as depicted in Scheme 4. Initially, our objective was to isolate the crucial chiral octahedral cobaltacycle intermediate implicated in the catalytic cycle.



Scheme 4. Mechanistic studies and control experiments.

The predominant diastereomer of the in situ-formed octahedral cobaltacycle, denoted as *mer*-[(S_L)-ΔCo], was successfully isolated in 39 % yield utilizing benzamide **1a** with Co(OAc)₂·4H₂O, (S)-L5, NaOPiv, Na₂EosinY, and 4-acetylpyridine in 2,2,2-trifluoroethanol (TFE) under air atmosphere for 36 hours (Scheme 4a). The structure and

stereochemistry of $mer-[(S_L)-\Delta Co]$ were corroborated via X-ray crystallography. Subsequently, employing the isolated cobaltacycle $mer-[(S_L)-\Delta Co]$ in a stoichiometric reaction with *N*-pyrimidyl indole furnished the desired product **3aa** in 70 % yield with 92 % enantiomeric excess (*ee*) (Scheme 4b). Furthermore, catalytic utilization of the octahedral cobaltacycle $mer-[(S_L)-\Delta Co]$ engendered the desired annulation product **3aa** in 21 % yield with 85 % *ee* (Scheme 4c). Both catalytic and stoichiometric experiments corroborated the involvement of the cobaltacycle $mer-[(S_L)-\Delta Co]$ in the catalytic cycle. To gain insights into the reaction pathway, we conducted the standard reaction in the presence of radical scavengers such as TEMPO and BHT, resulting in a significant reduction in product yield (10 % and 12 %, respectively), indicative of single electron transfer involvement during the catalytic cycle (see the Supporting Information).^[41] Furthermore, supplementation of the reaction mixture with 1.0 equiv. of DABCO did not affect the product yield, suggesting the absence of singlet oxygen during the reaction (Scheme 4d). To exclude the potential formation of superoxide anion via the photoredox process, the standard reaction was conducted in the presence of KO_2 under argon atmosphere, yielding only trace amounts of the desired product **3aa**, thus indicating that in situ-generation of O_2^- is insufficient to re-oxidize the low-valent cobalt species (Scheme 4e).

Subsequently, an intramolecular competitive experiment was conducted between electron-donating (**1o**) and electron-withdrawing (**1r**) substituents at the C-3 position of benzamide. Analysis revealed that substrate **1o** exhibited faster reactivity compared to **1r**, suggesting C–H bond activation occurs via Base-Induced Electrophilic Substitution (BIES) pathway.^[41]

Additionally, D/H scrambling experiments employing $[D_5]$ -**1a** in the absence and presence of *N*-pyrimidyl indole indicated significant D/H exchange at the ortho C–H bond in the recovered benzamide and annulated product,

indicative of reversible C–H activation and involvement of the concerted metalation-deprotonation (CMD) pathway in the catalytic cycle (Scheme 4f&4g). Moreover, a kinetic isotope effect value of 1.28 suggested that the C–H bond cleavage step of benzamide is not the rate-determining step (Scheme 4h).

DFT Studies

Quantum chemical investigations using density functional theory (DFT) were performed to gain further insights into reaction mechanism and the key energetics were depicted in Figure 1. The reference point for our calculations was $[(N,N-1a)(S_L)Co^{III}(\kappa^2-Piv)]$,^[41] with a transition state energy of 5.89 kcal/mol required to surpass the carboxylate-assisted concerted-metalation and deprotonation step. Upon C–H activation, multiple diastereomers are feasible. However, since the crystal structure confirmed meridional coordination modes as the geometrical isomer for the isolated cobalt complex, we did not compute the energy difference between these geometrical isomers. Given the fixed stereochemistry of the ligand with the use of enantiopure Salox ligand (**S**)-**L5**, we proceeded to evaluate the energy difference between the two principal optical isomers ($\Delta Co/\Lambda Co$). Upon cyclocobaltation, this analysis revealed a disparity of 11.44 kcal/mol, favoring the intermediate $mer-[(S_L)-\Delta Co]$. Subsequent substitution of pivalic acid with TFE in intermediate **D** demonstrated an energy barrier of 8.91 kcal/mol between the two optical isomers, thus reinforcing the superior stability of $mer-[(S_L)-\Delta Co]$.

Upon ligand exchange with indole in intermediate **D**, two stereoisomers $mer-[(S_L)(R,R)-\Delta Co]$ and $mer-[(S_L)(S,S)-\Delta Co]$ were formed depending on the orientation of the indole during migratory insertion. The transition state energy difference between these orientations was found to

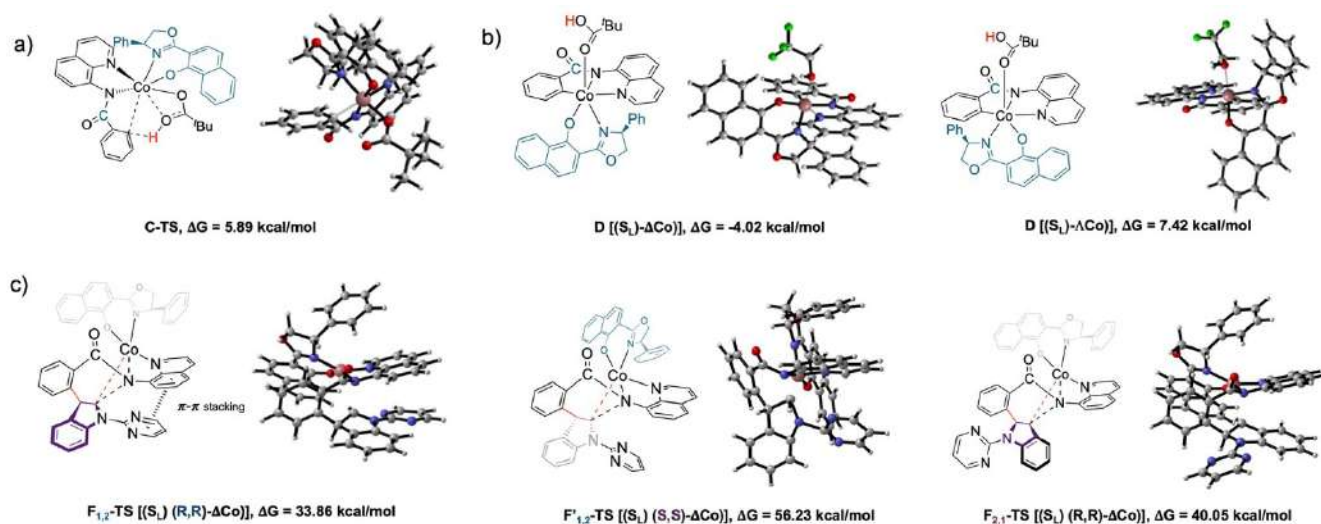


Figure 1. DFT calculations on (a) enantiodetermining C–H activation, (b) optimized structures for $mer-[(S_L)-\Delta Co]$ and $mer-[(S_L)-\Lambda Co]$ and (c) TS of the reductive elimination step.

be 4.96 kcal/mol. In the subsequent reductive elimination of intermediate **F** must pass through the transition state with the energy barrier of 33.87 kcal/mol for *mer*-[(*S_L*)-(*R,R*)- Δ Co] and 50.68 kcal/mol for *mer*-[(*S_L*)(*S,S*)- Δ Co], favoring **3aa**-(*R,R*) under the reaction conditions. The stabilization of F_{1,2}-TS, *mer*-[(*S_L*)(*R,R*)- Δ Co], was evident through π - π stacking between the pyrimidine ring and arene of the 8-aminoquinoline. These computational results align with our experimental outcomes, further confirmed by X-ray analysis of the isolated dearomatized annulation products (**3aa**, **3qa**, **3oa**, and **3ua**), establishing its absolute configuration as (*R,R*). Finally, the energy barrier for the 2,1-migratory insertion followed by reductive elimination was found to be 6.19 kcal/mol higher in energy compared to 1,2-migratory insertion, consistent with the experimental results as observed only 1,2-migratory insertion product from the reaction mixture. Overall, the energy profile suggests that reductive elimination, rather than C–H activation, is the rate-determining step, consistent with our experimental observations.

Drawing upon control experiments, stoichiometric studies, and DFT investigations, a plausible mechanistic pathway has been delineated, as shown in Scheme 5.^[36b,38–39] Initially, intermediate **B** is formed through sequential ligand exchange between Co(OAc)₂·4H₂O, (*S*)-Salox ligand, and benzamide **1a**, followed by one-electron oxidation yielding Co(III) intermediate **C**. Photoexcited Na₂Eosin Y* facilitates the oxidation of Co(II) to Co(III), generating a radical anion of Na₂Eosin Y as a potent reductant. This species may then reduce triplet oxygen present in the reaction, completing a parallel catalytic cycle. Subsequently, car-

boxylate-assisted enantiodetermining C–H activation provides the diastereoselective *mer*-[(*S_L*)- Δ Co] cobaltacycle **D**. Upon coordination with the π -bond of the pyrrole ring in the indole molecule, intermediate **D** undergoes subsequent regioselective insertion between Co–C, stabilized by π - π stacking of the pyrimidine ring with the arene of the quinoline, yielding intermediate **F**. Further, reductive elimination from intermediate **F** and subsequent ligand exchange leads to the formation of the desired product **3aa** and liberated Co(I) species subsequently couples with benzamide **1a**, followed by oxidation mediated by the photocatalyst, regenerating the Cobalt intermediate **B**.

Conclusion

In summary, we demonstrate the pioneering example of cobalt-catalyzed asymmetric dearomatization reaction via cascade C–H activation, leveraging the π -bond present in indole to access enantioenriched three-dimensional cyclic scaffolds in a single step under mild conditions. Notably, the developed method operates without the need for a metal oxidant, relying solely on oxygen as the oxidant and employing an organic dye as a photocatalyst under irradiation. Exploration of the scope of amides and indoles involved an examination of the tolerance of various functional groups under the established conditions. Control experiments and stoichiometric studies indicate that the enantiodetermining step is the C–H activation, which is reversible, though not rate-determining. Ongoing efforts in our laboratory are directed towards further harnessing this dual cobalt-photocatalytic approach for asymmetric functionalizations, promising to unveil novel synthetic methods and expand the repertoire of accessible chiral architectures.

Acknowledgements

Financial support provided by SERB (CRG/2020/001282) to support this research work is gratefully acknowledged. AD, SK and HSR acknowledges CSIR, IITK and PMRF for their fellowship.

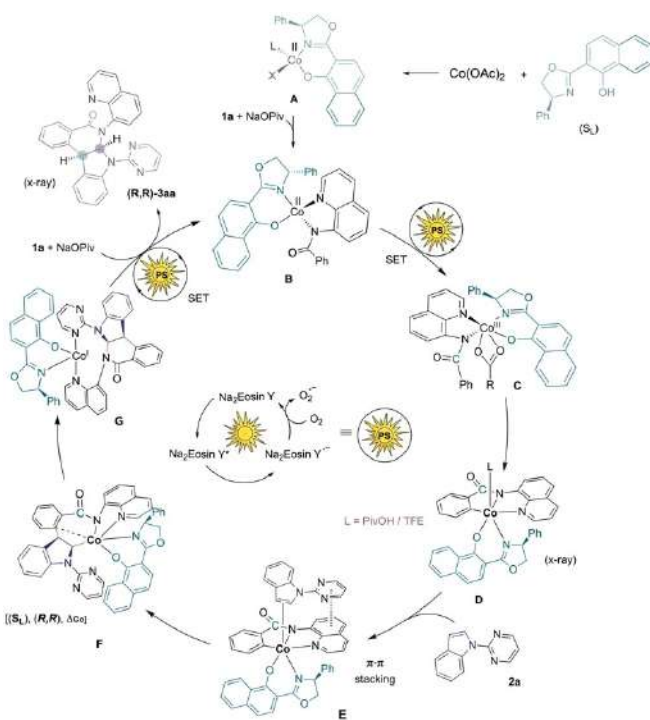
Conflict of Interest

The authors declare no conflict of interest.

Data Availability Statement

The data underlying this study are available in the published article and its Supporting Information.

Keywords: Dearomatization • C–H bond Functionalization • Cobalt • Indole • Photoredox • Asymmetric Catalysis



Scheme 5. Proposed mechanism.

- [1] R. Kaiser, *Angew. Chem. Int. Ed. Engl.* **1968**, *7*, 345–350.
- [2] C. Zheng, S.-L. You, *ACS Cent. Sci.* **2021**, *7*, 432–444.
- [3] W. C. Wertjes, E. H. Southgate, D. Sarlah, *Chem. Soc. Rev.* **2018**, *47*, 7996–8017.
- [4] C. J. Huck, D. Sarlah, *Chem* **2020**, *6*, 1589–1603.
- [5] C. Zheng, S.-L. You, *Chem* **2016**, *1*, 830–857.
- [6] P. V. R. Schleyer, H. Jiao, *Pure Appl. Chem.* **1996**, *68*, 209–218.
- [7] M. Randic, *Chem. Rev.* **2003**, *103*, 3449–3606.
- [8] Y. Hua, H. Zhang, H. Xia, *Chin. J. Org. Chem.* **2018**, *38*, 11–28.
- [9] D. Astruc, *Ed. Modern Arene Chemistry: Concepts, Synthesis, and Applications*, Wiley-VCH **2002**.
- [10] J. Mortier, *Ed. Arene Chemistry: Reaction Mechanisms and Methods for Aromatic Compounds*, Wiley-VCH **2015**.
- [11] S. P. Roche, J. A. Porco Jr, *Angew. Chem. Int. Ed.* **2011**, *50*, 4068–4093.
- [12] C. Zheng, S.-L. You, *Nat. Prod. Rep.* **2019**, *36*, 1589–1605.
- [13] A. J. Birch, *Pure Appl. Chem.* **1996**, *68*, 553–556.
- [14] M. M. Heravi, M. V. Fard, Z. Faghihi, *Curr. Org. Chem.* **2015**, *19*, 1491–1525.
- [15] B. K. Peters, K. X. Rodriguez, S. H. Reisberg, S. B. Beil, D. P. Hickey, Y. Kawamata, M. Collins, J. Starr, L. Chen, S. Udyavara, K. Klunder, T. J. Gorey, S. Anderson, M. Neurock, S. D. Minter, P. S. Baran, *Science* **2019**, *363*, 838–845.
- [16] A. Chatterjee, B. König, *Angew. Chem. Int. Ed.* **2019**, *58*, 14289–14294.
- [17] K. Kondo, K. Kubota, H. Ito, *Chem. Sci.* **2024**, DOI: 10.1039/D3SC06052G.
- [18] Selected examples using Hydrogenation: a) M. Heitbaum, R. Fröhlich, F. Glorius, *Adv. Synth. Catal.* **2010**, *352*, 357–362; b) Y. Wei, B. Rao, X. Cong, X. Zeng, *J. Am. Chem. Soc.* **2015**, *137*, 9250–9253; c) R. Kuwano, R. Morioka, M. Kashiwabara, N. Kameyama, *Angew. Chem. Int. Ed.* **2012**, *51*, 4136–4139; d) M. P. Wiesenfeldt, Z. Nairoukh, W. Li, F. Glorius, *Science* **2017**, *357*, 908–912.
- [19] Selected examples on Dearomatization: a) Y. Schmidt, J. K. Lam, H. V. Pham, K. N. Houk, C. D. Vanderwal, *J. Am. Chem. Soc.* **2013**, *135*, 7339–7348; b) W. B. Motherwell, A. S. Williams, *Angew. Chem. Int. Ed. Engl.* **1995**, *34*, 2031–2033; c) B. M. Trost, V. Ehmke, B. M. O’Keefe, D. A. Bringley, *J. Am. Chem. Soc.* **2014**, *136*, 8213–8216; d) J. Ling, S. Lam, K.-H. Low, P. Chiu, *Angew. Chem. Int. Ed.* **2017**, *56*, 8879–8882; e) G. Jacquemot, M.-A. Ménard, C. L’Homme, S. Canesi, *Chem. Sci.* **2013**, *4*, 1287–1292; f) S. E. Reisman, R. R. Nani, S. Levin, *Synlett* **2011**, 2437–2442.
- [20] S. E. Lewis, *Asymmetric Dearomatization under Enzymatic Conditions*, Ed. S.-L. You, Wiley-VCH, **2016**, pp. 279–346.
- [21] Q. Cheng, Y. Wang, S.-L. You, *Angew. Chem. Int. Ed.* **2016**, *55*, 3496–3499.
- [22] H.-F. Tu, C. Zheng, R.-Q. Xu, X.-J. Liu, S.-L. You, *Angew. Chem. Int. Ed.* **2017**, *56*, 3237–3241.
- [23] D. Shen, Q. Chen, P. Yan, X. Zeng, G. Zhong, *Angew. Chem. Int. Ed.* **2017**, *56*, 3242–3246.
- [24] M. Aleksiev, O. García Mancheño, *Chem. Commun.* **2023**, *59*, 3360–3372.
- [25] C.-X. Zhuo, C. Zheng, S.-L. You, *Acc. Chem. Res.* **2014**, *47*, 2558–2573.
- [26] a) M. Okumura, D. Sarlah, *Synlett* **2018**, *29*, 845–855; b) K. Ikeda, R. Kojima, K. Kawai, T. Murakami, T. Kikuchi, M. Kojima, T. Yoshino, S. Matsunaga, *J. Am. Chem. Soc.* **2023**, *145*, 9326–9333; c) S. Pradhan, F. Mohammadi, J. Bouffard, *J. Am. Chem. Soc.* **2023**, *145*, 12214–12223.
- [27] a) J. Zheng, S.-B. Wang, C. Zheng, S.-L. You, *J. Am. Chem. Soc.* **2015**, *137*, 4880–4883; b) C. Zheng, J. Zheng, S.-L. You, *ACS Catal.* **2016**, *6*, 262–271.
- [28] X. Li, L. Hu, S. Ma, H. Yu, G. Lu, T. Xu, *ACS Catal.* **2023**, *13*, 4873.
- [29] a) S. Rej, A. Das, N. Chatani, *Coord. Chem. Rev.* **2021**, *431*, 213683; b) T. Rogge, N. Kaplaneris, N. Chatani, J. Kim, S. Chang, B. Punji, L. L. Schafer, D. G. Musaev, J. Wencel-Delord, C. A. Roberts, R. Sarpong, Z. E. Wilson, M. A. Brimble, M. J. Johansson, L. Ackermann, *Nat. Rev. Methods Primers* **2021**, *1*, 43; c) U. Dutta, S. Maiti, T. Bhattacharya, D. Maiti, *Science* **2021**, *372*, eabd5992 and references therein.
- [30] L. Grigorjeva, O. Daugulis, *Angew. Chem. Int. Ed.* **2014**, *53*, 10209–10212.
- [31] a) Y. Kommagalla, N. Chatani, *Coord. Chem. Rev.* **2017**, *350*, 117–135; b) L. Lukasevics, A. Cizikovs, L. Grigorjeva, *Chem. Commun.* **2021**, *57*, 10827–10841; c) A. Bacalini, S. Vergura, P. Dolui, G. Zanoni, D. Maiti, *Org. Biomol. Chem.* **2019**, *17*, 10119–10141; d) R. Mandal, B. Garai, B. Sundararaju, *Sci. Synth.* **2023**, *2*, 149–260.
- [32] a) P. Gandeevan, L. H. Finger, T. H. Meyer, L. Ackermann, *Chem. Soc. Rev.* **2020**, *49*, 4254–4272; b) V. Dwivedi, D. Kalsi, B. Sundararaju, *ChemCatChem* **2019**, *11*, 5160–5187; c) L. Guillemard, J. Wencel-Delord, *Beilstein J. Org. Chem.* **2020**, *16*, 1754–1804; d) P. Chakraborty, R. Mandal, S. Paira, B. Sundararaju, *Chem. Commun.* **2021**, *57*, 13075–13083.
- [33] A. Cizikovs, L. Grigorjeva, *Inorganics* **2023**, *11*, 194.
- [34] a) Y. Zheng, C. Zheng, Q. Gu, S.-L. You, *Chem. Catal.* **2022**, *2*, 2965–2985; b) B. Garai, A. Das, D. Vineet Kumar, B. Sundararaju, *Chem. Commun.* **2024**, *60*, 3354–3369; c) X. Yu, Z.-Z. Zhang, J.-L. Niu, B.-F. Shi, *Org. Chem. Front.* **2022**, *9*, 1458–1484.
- [35] Selected reviews on enantioselective C–H bond functionalizations with 3d metals, see: a) L. Woźniak, N. Cramer, *Trends Chem.* **2019**, *1*, 471–478; b) J. Loup, U. Dhawa, F. Pesciaoli, J. Wencel-Delord, L. Ackermann, *Angew. Chem. Int. Ed.* **2019**, *58*, 12803–12818; c) R. Mandal, B. Garai, B. Sundararaju, *ACS Catal.* **2022**, *12*, 3452–3506; d) T. Yoshino, *Bull. Chem. Soc. Jpn.* **2022**, *95*, 1280–1288; e) T. Yoshino, S. Matsunaga, *Synlett* **2019**, *30*, 1384–1400.
- [36] a) X.-J. Si, D. Yang, M.-C. Sun, D. Wei, M.-P. Song, J.-L. Niu, *Nat. Synth.* **2022**, *1*, 709–718; b) Q.-J. Yao, F.-R. Huang, J.-H. Chen, M.-Y. Zhong, B. F. Shi, *Angew. Chem. Int. Ed.* **2023**, *62*, e202218533; c) D. Yang, X. Zhang, X. Wang, X.-J. Si, J. Wang, D. Wei, M.-P. Song, J.-L. Niu, *ACS Catal.* **2023**, *13*, 4250–4260; d) Z.-K. Wang, Y.-J. Wu, Q.-J. Yao, B.-F. Shi, *Angew. Chem. Int. Ed.* **2023**, *62*, e202304706; e) T. Li, L. Shi, X. Wang, C. Yang, D. Yang, M.-P. Song, J.-L. Niu, *Nat. Commun.* **2023**, *14*, 527; f) Y.-J. Wu, J.-H. Chen, M.-Y. Teng, X. Li, T.-Y. Jiang, F.-R. Huang, Q.-J. Yao, B.-F. Shi, *J. Am. Chem. Soc.* **2023**, *145*, 24499–24505; g) Y.-J. Wu, Z.-K. Wang, Z.-S. Jia, J.-H. Chen, F.-R. Huang, B.-B. Zhan, Q.-J. Yao, B.-F. Shi, *Angew. Chem. Int. Ed.* **2023**, *62*, e2023100; h) Y. Lin, T. von Münchow, L. Ackermann, *ACS Catal.* **2023**, *14*, 9713–9723; i) M.-Y. Teng, Y.-J. Wu, J.-H. Chen, F.-R. Huang, D.-Y. Liu, Q.-J. Yao, B.-F. Shi, *Angew. Chem. Int. Ed.* **2024**, *63*, e2023188.
- [37] a) Q.-J. Yao, J.-H. Chen, H. Song, F.-R. Huang, B.-F. Shi, *Angew. Chem. Int. Ed.* **2022**, *61*, e202202892; b) J.-H. Chen, M.-Y. Teng, F.-R. Huang, H. Song, Z.-K. Wang, H.-L. Zhuang, Y.-J. Wu, X. Wu, Q.-J. Yao, B.-F. Shi, *Angew. Chem. Int. Ed.* **2022**, *61*, e202210106; c) T. von Münchow, S. Dana, Y. Xu, B. Yuan, L. Ackermann, *Science* **2023**, *379*, 1036–1042; d) G. Zhou, J.-H. Chen, Q.-J. Yao, F.-R. Huang, Z.-K. Wang, B.-F. Shi, *Angew. Chem. Int. Ed.* **2023**, *62*, e202302964; e) T. Liu, W. Zhang, C. Xu, Z. Xu, D. Song, W. Qian, G. Lu, C.-J. Zhang, W. Zhong, F. Ling, *Green Chem.* **2023**, *25*, 3606–3614; f) A. Das, R. Mandal, H. S. Ravi sankar, S. Kumaran, D. Borah, J. R. Premkumar, B. Sundararaju, *Angew. Chem. Int. Ed.* **2024**, *63*, e202315005.
- [38] a) D. Kalsi, S. Dutta, N. Barsu, M. Rueping, B. Sundararaju, *ACS Catal.* **2018**, *8*, 8115–8120; b) D. Kalsi, N. Barsu, S. Chakrabarti, P. Dahiya, M. Rueping, B. Sundararaju, *Chem.*

- Commun.* **2019**, 55, 11626–11629; c) R. Mandal, N. Barsu, B. Garai, A. Das, D. Perekalin, B. Sundararaju, *Chem. Commun.* **2021**, 57, 13075–13083.
- [39] For contribution from other research groups, see: a) Y.-L. Ban, L. You, T. Wang, L.-Z. Wu, Q. Liu, *ACS Catal.* **2021**, 11, 5054–5060; b) S. Kumar, A. M. Nair, C. M. R. Volla, *Chem. Asian J.* **2022**, 17, e202200801; c) N. P. Khot, N. K. Deo, M. Kapur, *Chem. Commun.* **2022**, 58, 13967–13970; d) C. Sen, B. Sarvaiya, S. Sarkar, S. C. Ghosh, *J. Org. Chem.* **2020**, 23, 15287–15304.
- [40] CCDC 2344417 (**3aa**), 2344418 (**3oa**), 2344419 (**3qa**), 2344420 (**3ua**), and CCDC 2344416 *mer*-[(S_L)- Δ Co] contains the

supplementary crystallographic data for this paper. These data can be obtained free of charge from The Cambridge Crystallographic Data Centre via www.ccdc.cam.ac.uk/data_request/cif. The Supporting Information also provides additional information.

[41] See the Supporting Information for more details.

Manuscript received: April 1, 2024

Accepted manuscript online: June 19, 2024

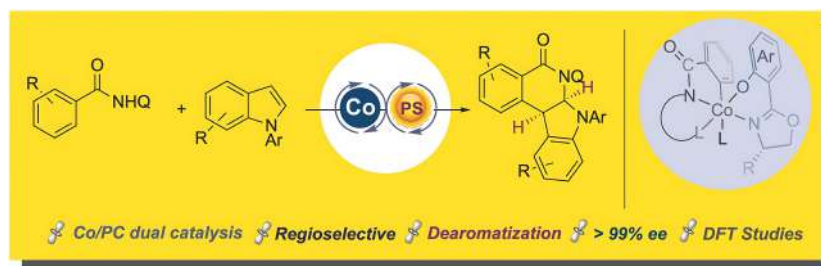
Version of record online: ■■, ■■

Research Article

Asymmetric Catalysis

A. Das, S. Kumaran, H. S. Ravi Sankar,
J. R. Premkumar,
B. Sundararaju* _____ e202406195

A Dual Cobalt-Photoredox Catalytic Approach for Asymmetric Dearomatization of Indoles with Aryl Amides via C–H Activation



In this study, we showcase cobalt-catalyzed asymmetric dearomatization of indoles with aryl amides, achieving remarkable enantioinduction and exceptional regioselectivity. This dual catalytic strategy, which integrates photocatalyst

and cobalt, represents a pioneering approach in asymmetric C–H bond functionalization. Through detailed experimental investigations and DFT calculations, we present a plausible mechanism to elucidate the reaction pathway.

Asymmetric Catalysis

Reversal of Regioselectivity in Asymmetric C–H Bond Annulation with Bromoalkynes under Cobalt Catalysis**

Abir Das, Rajib Mandal, Harihara Subramanian Ravi Sankar, Subramani Kumaran, J. Richard Premkumar, Dipanti Borah, and Basker Sundararaju*

Abstract: Metal-catalyzed asymmetric C–H bond annulation strategy offers a versatile platform, allowing the construction of complex P-chiral molecules through atom- and step-economical fashion. However, regioselective insertion of π -coupling partner between M–C bond with high enantio-induction remain elusive. Using commercially available Co(II) salt and chiral-Salox ligands, we demonstrate an unusual protocol for the regio-reversal, enantioselective C–H bond annulation of phosphinamide with bromoalkyne through desymmetrization. The reaction proceeds through ligand-assisted enantiodetermining cyclocobaltation followed by regioselective insertion of bromoalkyne between Co–C, subsequent reductive elimination, and halogen exchange with carboxylate resulted in P-stereogenic compounds in excellent *ee* (up to >99 %). The isolation of cobaltacycle involved in the catalytic cycle and the outcome of control experiments provide support for a plausible mechanism.

extensively with 4d and 5d metals, as the reaction not only atom and step-economical but also very useful in creating chiral molecules in one step from the C–H bonds.^{[3][4]} In spite of the notable developments over the last decade, and in light of the alarming depletion of those metals on the Earth's crust, a surge has recently been realized in carrying out enantioselective C–H functionalization with abundant 3d metal catalysts.^[5] In this regard, high-valent cobalt catalysis has been shown to be of significant interest among other 3d metals due to its distinct reactivity in comparison to that of 4d and 5d metals.^[6]

Within high-valent cobalt-catalyzed asymmetric C–H bond functionalizations, a couple of interesting strategies have been explored as shown in Scheme 1a.^[7–10] Cramer and co-workers developed tailor made chiral cyclopentadienyl-based cobalt(III) catalysts for the enantioselective annulation of *N*-chlorobenzamides with alkenes in 2019, and the strategy was further extended to enantioselective C–H alkylation.^[7] During the same time, Ackermann,^[8] Matsunaga^[9] and Shi^[10] independently developed a hybrid catalytic system that combines chiral carboxylic acid (CCA) with achiral Cp*Co(III) catalyst. It has been shown that

Introduction

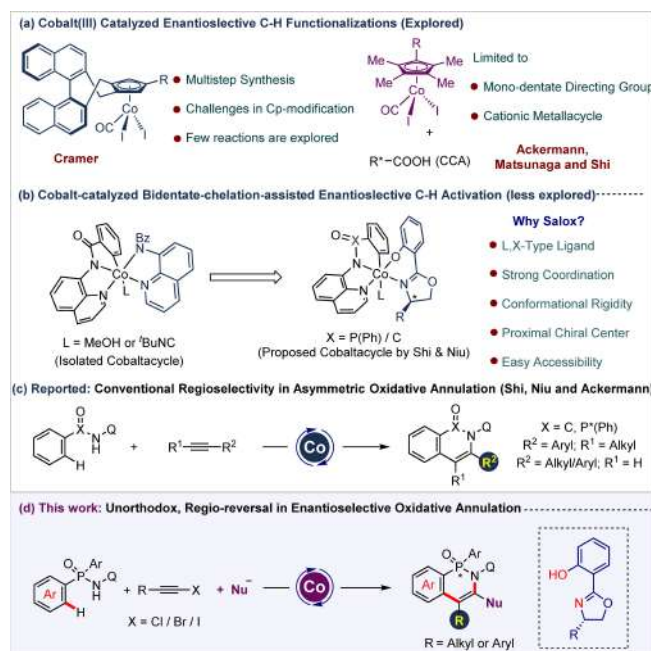
Synthesis of organic molecules with high optical purity is essential for synthetic chemists due to the prevalence of chiral components in the pharmaceutical and agrochemical industries.^[1] As a result, enantioselective catalysis has made tremendous strides forward over the course of the years; however, the effort to design chiral systems that are more effective in producing high levels of enantioinduction continues unabated.^[2] In this regard, direct, one-step asymmetric C–H bond functionalization has been explored

[*] A. Das, R. Mandal, H. S. Ravi Sankar, Dr. S. Kumaran, Prof. Dr. B. Sundararaju
Department of Chemistry, Indian Institute of Technology Kanpur
208016 Kanpur, Uttar Pradesh (India)
E-mail: basker@iitk.ac.in

Dr. J. R. Premkumar
PG & Research Department of Chemistry, Bishop Heber College
620017 Tiruchirappalli, Tamil Nadu (India)

D. Borah
Department of Chemistry, Indian Institute of Technology Bombay
Powai, 400076 Mumbai, Maharashtra (India)

[**] A previous version of this manuscript has been deposited on a preprint server (<https://doi.org/10.26434/chemrxiv-2023-1rqz1>).



Scheme 1. Overview of Ligand enabled Co(III) catalysis and asymmetric C–H bond functionalizations.

enantioselective C(sp²)-H and C(sp³)-H functionalizations can be achieved with both chiral cyclopentadienyl and hybrid catalytic strategies. However, there are still impediments to their widespread use such as the time-consuming and laborious multistep synthesis of the former, and the latter necessitates the generation of cationic cobaltacycle in hybrid strategies involving CCA (Scheme 1a).

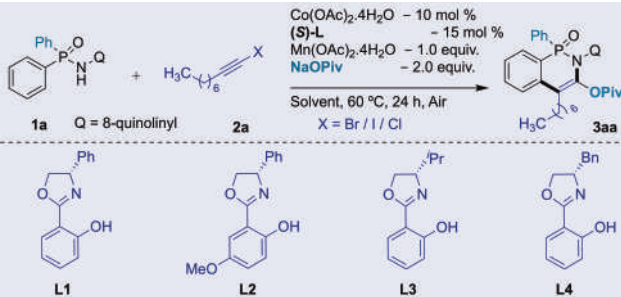
Meanwhile, a Cp*-free, bidentate-chelation-assistance approach that was pioneered by Daugulis and co-workers has displayed widespread application over the years owing to the use of commercially available Co(II) and Co(III) salts as precatalysts.^[11] However, mechanistic aspects such as the coordination environment around the cobalt were a subject of intense speculation until the octahedral cobaltacycle was isolated.^[12] It was discovered that the process of functionalization requires the participation of two 8-aminoquinoline moieties as L,X-type ligand bound to cobalt. One of these moieties is present in the substrate and brings the metal in close-proximity to the C-H bond, while the other acts as a spectator ligand. The resultant cobalt(III)-metallacycle obtained in octahedral geometry where the sixth coordination site is bound with solvent or labile ligand (Scheme 1b). To further exploit the scope of cobalt(II)-bidentate directed catalysis in asymmetric C-H bond functionalization, Shi and Niu independently developed oxidative asymmetric C-H bond annulation of aryl amides/phosphinamides with alkynes using chiral Salox as an external ligand assisted by 8-aminoquinoline (AQ) as bidentate directing group.^[13] Later, Shi, Ackermann, Niu independently reported asymmetric electro-cobalt catalysis for oxidative C-H and N-H bond annulation of amides with alkynes and alkenes using electricity as oxidant.^[14]

The above-mentioned asymmetric C-H and N-H bond annulation reactions with alkynes follow the traditional regioselective annulation mechanism, in which the aryl group of the aryl-alkyl alkyne and the aryl/alkyl substituent attached in the terminal alkyne prefer to be close to the 'N' atom of the amide (α -carbon to the N-atom) (Scheme 1c). We hypothesized that by changing the polar groups attached to the alkyne stem can potentially reverse the regioselective migratory insertion between Co-C, resulting in an inverse-regioselective annulation product (alkyl group β -carbon to the N-atom).^[15] To test our hypothesis and continue our efforts to develop cobalt catalyzed C-H functionalizations,^[16] we attempted to access such scaffolds via cobalt(II)/(S)-Salox catalyzed enantioselective C-H and N-H bond annulation phosphinamides with bromoalkynes, which were primarily investigated for C-H alkynylation. It is hoped that using bromoalkyne as a coupling partner will change the regioselectivity of the conventional oxidative annulation of amide. Furthermore, the bromo functionality may engage with suitable soft nucleophile in situ, resulting in the formation of a complex molecular framework in a single step.

Results and Discussion

Our investigation of the untapped potential of bromoalkynes in cobalt-catalyzed enantioselective oxidative annulation began with the reaction of *P,P*-diphenyl-N-(quinoline-8-yl)phosphinic amide **1a** with 2-bromonon-1-yne **2a** as model substrate in TFE (0.2 M) at 60 °C for 24 hours in the presence of 10 mol % Co(OAc)₂·4H₂O, 15 mol % (S)-Salox (**L1**) (Table 1). C3-oxygenated *P*-stereogenic product **3aa** with perfect inverse regioselectivity was produced as a single regioisomer with 39 % yield and 59 % *ee* as intended (Entry 1). Unlike other internal alkynes, we neither observe mixture of regioisomers nor any C-H alkynylation product, when bromoalkyne **2a** was employed as internal alkyne. To improve enantioselectivity and yield, solvents and chiral Salox ligands were screened (entries 2–7). Among the several solvents examined, *tert*-butanol was found to be the most effective for C-H annulation with good *ee* (entries 1–4). A quick screening of stereo-electronically modified chiral Salox ligands (derived from optically pure amino acids^[17]) revealed (S)-**L4** as the best chiral ligand with 72 % yield and

Table 1: Reaction optimization.^[a]



Entry	L	Base	Solvent	Yield (%) ^[b]	<i>ee</i> (%) ^[c]
1	(S)-L1	NaOPiv	TFE	39	59
2	(S)-L1	NaOPiv	EtOH	Trace	n.d.
3	(S)-L1	NaOPiv	Dioxane	Trace	n.d.
4	(S)-L1	NaOPiv	^t BuOH	93	89
5	(S)-L2	NaOPiv	^t BuOH	Trace	n.d.
6	(S)-L3	NaOPiv	^t BuOH	51	98
7	(S)-L4	NaOPiv	^t BuOH	72	97
8	(S)-L4	NaOPiv	^t BuOH	92	98 ^[d]
9	(S)-L4	Piv-OH	^t BuOH	Trace	n.d. ^[d]
10	–	NaOPiv	^t BuOH	n.r.	n.d. ^[d]
11	(S)-L4	–	^t BuOH	n.r.	n.d. ^[d]
12	(S)-L4	NaOPiv	^t BuOH	n.r.	n.d. ^[d,e]
13	(S)-L4	NaOPiv	^t BuOH	n.r.	n.d. ^[d,f]
14	(S)-L4	NaOPiv	^t BuOH	74	99 ^[d,g]
15	(S)-L4	NaOPiv	^t BuOH	77	99 ^[d,h]
16	(S)-L4	NaOPiv	^t BuOH	82	99 ^[d,i]

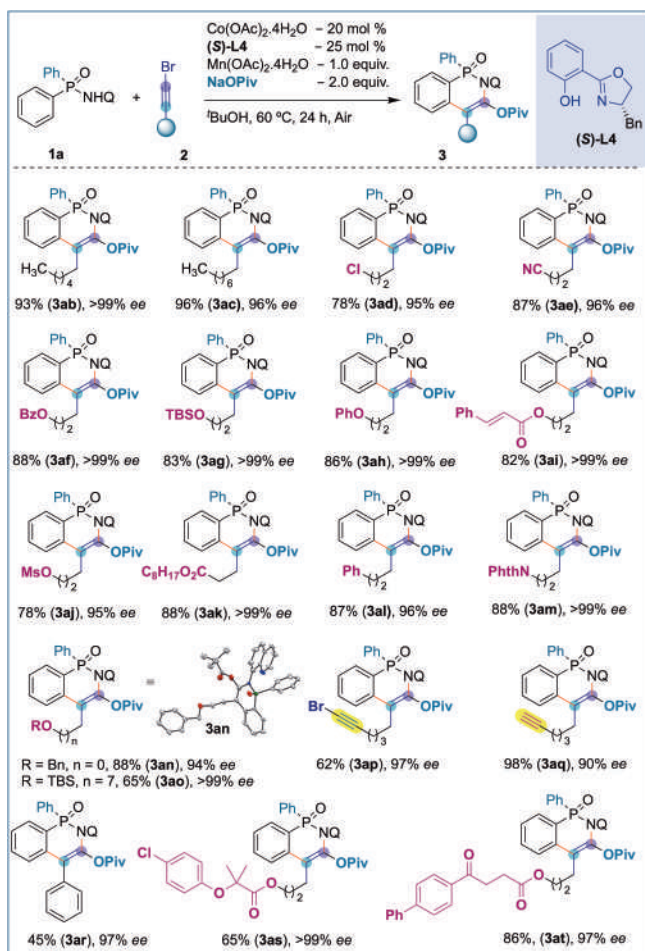
[a] All reactions were carried out under air unless otherwise stated using **1a** (0.1 mmol), **2a** (0.15 mmol), Co(OAc)₂·4H₂O (10 mol %), Salox **L** (15 mol %), NaOPiv (0.20 mmol) and Mn(OAc)₂·4H₂O (0.1 mmol) in ^tBuOH (0.5 mL) at 60 °C for 24 h. [b] Isolated yield. [c] The *ee* values were determined by chiral HPLC analysis. [d] 20 mol % of Co(OAc)₂·4H₂O and 25 mol % of (S)-**L4** used. [e] without Co(OAc)₂·4H₂O [f] without Mn(OAc)₂·4H₂O [g] Reaction performed in 1.0 mmol scale. [h] alkynyl iodide was used in place of **2a**. [i] alkynyl chloride was used in place of **2a**. TFE = 2,2,2-Trifluoroethanol, n.r. = no reaction, n.d. = not determined.

97 % *ee* (entries 4–7). Further increase of catalyst loading to 20 mol % led to 92 % isolated yield of **3aa** with 98 % *ee* (entry 8). However, change of carboxylate from pivalate to pivalic acid did not provide any product formation inferring the carboxylate play a vital role in cobaltacycle formation (entry 9). Control experiments revealed that the reaction failed to yield the desired outcome in the absence of the catalyst, base, oxidant, ligand, or change of the directing group^[18] (Entries 10–13). The reaction was performed at a scale of 1.0 mmol to evaluate the scalability of the developed protocol, and it produced the intended product with a yield of 74 % with 99 % *ee*. (Entry 14). There was no change in the reaction outcome when bromoalkyne is replaced with iodo/chloroalkyne under the optimized conditions (entries 15–16).

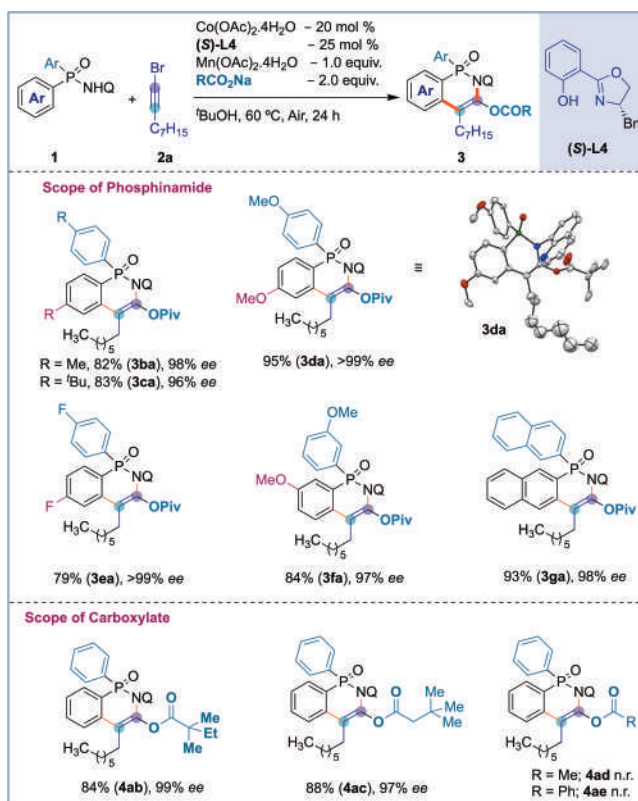
The scope of bromoalkynes was then investigated as shown in Scheme 2. Various substituted bromoalkynes **2** were suitable under the given conditions, resulting in the desired products (**3ab–3an**) with good-to-excellent yields (78–96 %) and a high level of enantioinduction (up to >99.0 % *ee*). The structure of **3an** was determined using X-ray crystallography and the absolute stereochemistry is assigned as *S*-configuration from the data obtained.^[19] To further ascertain our results, **2n** was subjected to oxidative

annulation with (*R*)-Salox ligand ((*R*)-**L4**) instead of (*S*)-variant, and the HPLC analysis suggest that the opposite isomer, i.e., (*R*) isomer of **3an** was obtained in 99 % *ee*. Functional groups such as –Cl, –CN, –OCO₂R, –OPh, and –OTBS were unaffected under the optimized conditions, allowing them to act as an additional handle for post-synthetic modifications. The chain length of bromoalkynes did not alter the enantioselectivity, demonstrating that the approach is applicable to a broad variety of bromoalkynes (**3ao** vs **3ag**). Furthermore, selective monoannulation was achieved with 1,7-dibromohepta-1,6-diyne, yielding **3ap** with excellent enantioselectivity (97 % *ee*). Bromoalkyne tethered terminal alkyne underwent selective annulation at the internal alkyne, yielding the desired product **3aq** with high yield (98 %) and enantioselectivity (90 % *ee*) while leaving the terminal alkyne unaffected. Encouragingly, the challenging phenyl alkynyl bromide **2r** was tolerated, harnessing the product **3ar** with desired selectivity in acceptable yield and excellent enantioinduction. To further expand the application of the protocol, biologically relevant bromoalkynes (**2s** & **2t**) were synthesized from drugs used to treat high cholesterol and inflammation, such as clofibric acid and fenbufen. The bromoalkynes derived from both the molecules furnished the annulated products (**3as** & **3at**) without compromise in the yield and enantioselectivity.

Next, the suitability of stereo electronically biased diarylphosphinamides for desymmetrization process was explored (Scheme 3). Various electron-donating and electron-withdrawing *para*-substituted phosphinamides **1b–1d** were found



Scheme 2. Scope of alkynyl bromides.

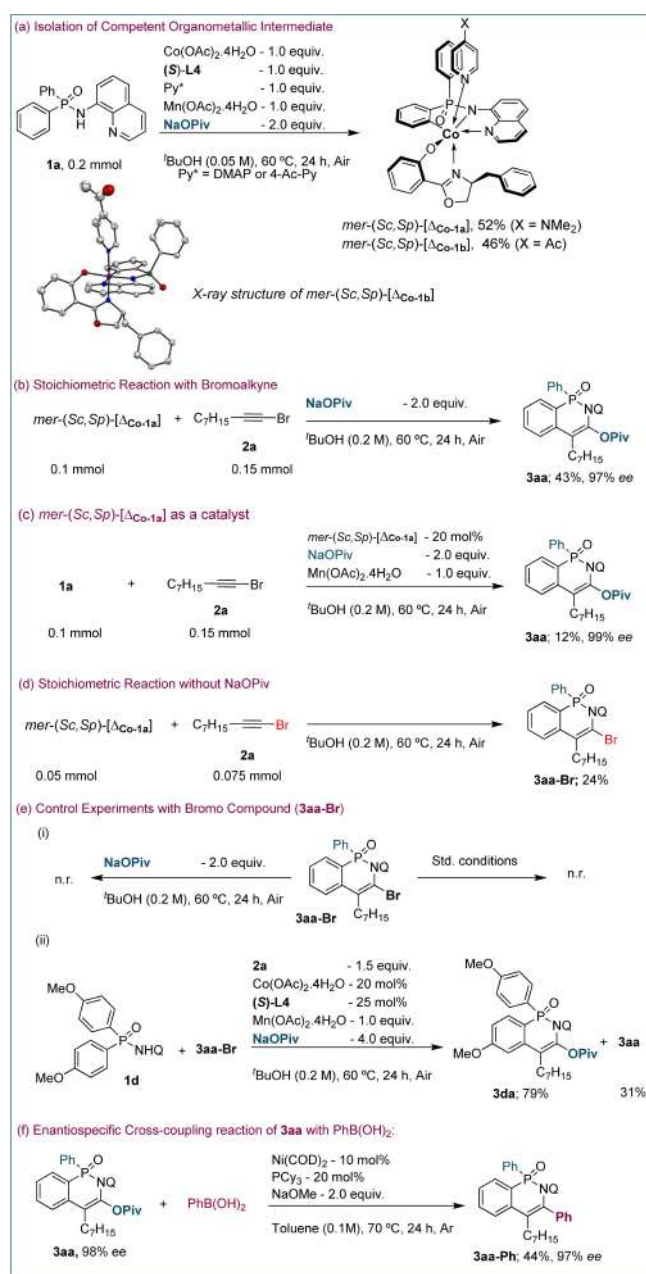


Scheme 3. Scope of phosphinamides and carboxylates.

to be amenable to the annulation process with the yield in the ranges of 79–82 %, and enantioselectivity in the range of 94–> 99 % *ee* (**3ba–3ea**). The structure and stereochemistry of **3da** is further confirmed through X-ray crystallography.^[19] While the meta-substituted diarylphosphinamides were subjected for annulation resulted in C–H bond functionalization at the less-hindered ortho-site in 84 % yield (**3fa**) with 97 % *ee*. Moreover, sterically-hindered bisnaphthyl phosphinamide **3ga** smoothly underwent the desired annulation at C-3 position over C-1, providing the desired product in excellent *ee*. Additionally, the extent of the sodium carboxylate additives was examined. Sodium carboxylate derived from 2,2-dimethylbutanoic acid and 3,3-dimethylbutanoic acid underwent annulation smoothly to access the respective products (**4ab** & **4ac**) without compromise in mass of the product and *ee*. However, no reaction was observed when less nucleophilic sodium acetate and sodium benzoate were used as carboxylate source (**4ad** & **4ae**).

To understand the reaction mechanism, various control experiments and DFT calculations were conducted (Scheme 4). At first, a stoichiometric reaction was carried out under the reported conditions^[13a] using phosphinamide **1a** with $\text{Co}(\text{OAc})_2 \cdot 4\text{H}_2\text{O}$, $\text{Mn}(\text{OAc})_2 \cdot 4\text{H}_2\text{O}$, (*S*)-**L4**, NaOPiv, and pyridine derivative in *t*-BuOH under air, furnishing an chiral octahedral cobaltacycle *mer*-(*Sc,Sp*)-[$\Delta_{\text{Co-1a}}$] (with DMAP) as a major diastereomer in 52 % and *mer*-(*Sc,Sp*)-[$\Delta_{\text{Co-1b}}$] 46 % (with 4-acetylpyridine) isolated yields (Scheme 4(a)). The spectroscopic data of isolated cobalt complexes *mer*-(*Sc,Sp*)-[$\Delta_{\text{Co-1}}$] is in line with the reported cobaltacycle.^[13] The structure of the *mer*-(*Sc,Sp*)-[$\Delta_{\text{Co-1b}}$] is further confirmed by X-ray crystallography.^[19] There are several optical isomers are possible for the resultant cobaltacycle namely, chirality on the ligand (*Sc*), phosphorus atom become chiral upon C–H activation (*Sp* and *Rp*) and the two possible propeller orientations of the octahedral cobalt-(III) complexes [$\Delta_{\text{Co-1}}$ and $\Lambda_{\text{Co-1}}$]. Since, we have taken the enantiopure ligand, we move on to check the energetics of other chiral centers through DFT calculation. At first, the DFT studies were performed for the carboxylate-assisted C–H bond activation starting from carboxylate bound octahedral complex. The enantioselective C–H bond activation may proceed through two possible transition state based on phosphorus namely, TS-(*Sp*) and TS-(*Rp*) and the subsequent cobaltacycle will provide the (*S*) or (*R*)-products. The difference in energy between TS-(*Sp*) orientation is found to be 22.66 kJ/mol lower in energy compared to the TS-(*Rp*) of the phosphorus suggesting that the (*S*) isomer is more favoured and the theoretically predicted *ee* is found to be 99.9 % (Figure 1a). These results further confirming the stereochemical confirmation of the final product and our experimentally observed *ee* is in line with theoretical studies (Figure 1a).^[18] We then calculate the energy difference between *mer*-(*Sc,Sp*)-[$\Delta_{\text{Co-1}}$] and *mer*-(*Sc,Sp*)-[$\Lambda_{\text{Co-1}}$], and the results suggest that the former is 52.16 kJ/mol lower in energy than the latter orientations (Figure 1b).^[18]

We next performed the calculation on the migratory insertion step to rationalize the reason to obtain single regioisomer. The migratory insertion of 1,2-insertion vs 2,1-



Scheme 4. Mechanistic investigations and derivatization.

insertion pathway with octahedral cobaltacycle *mer*-(*Sc,Sp*)-[$\Delta_{\text{Co-1}}$] is calculated both singlet states and in triplet states. The relative free energy of the two transition states differs by 14.55 kJ/mol resulting in favor of 1,2-insertion over the 2,1-insertion (Figure 1c).^[18] These results indicates that the 1,2-migratory insertion pathway is the preferred over the 2,1-migratory insertion pathway. To further validate our theoretical results, we performed the stoichiometric experiment between the cobaltacycle *mer*-(*Sc,Sp*)-[$\Delta_{\text{Co-1a}}$] and bromoalkynes **2a** in the presence of sodium pivalate in *tert*-butanol, yielding the desired product **3aa** in 43 % yield and 99 % *ee* (Scheme 4b), and the absolute configuration **3aa** is similar to the one structurally assigned for **3an**. Thereafter, the octahedral complex *mer*-(*Sc,Sp*)-[$\Delta_{\text{Co-1a}}$] was employed

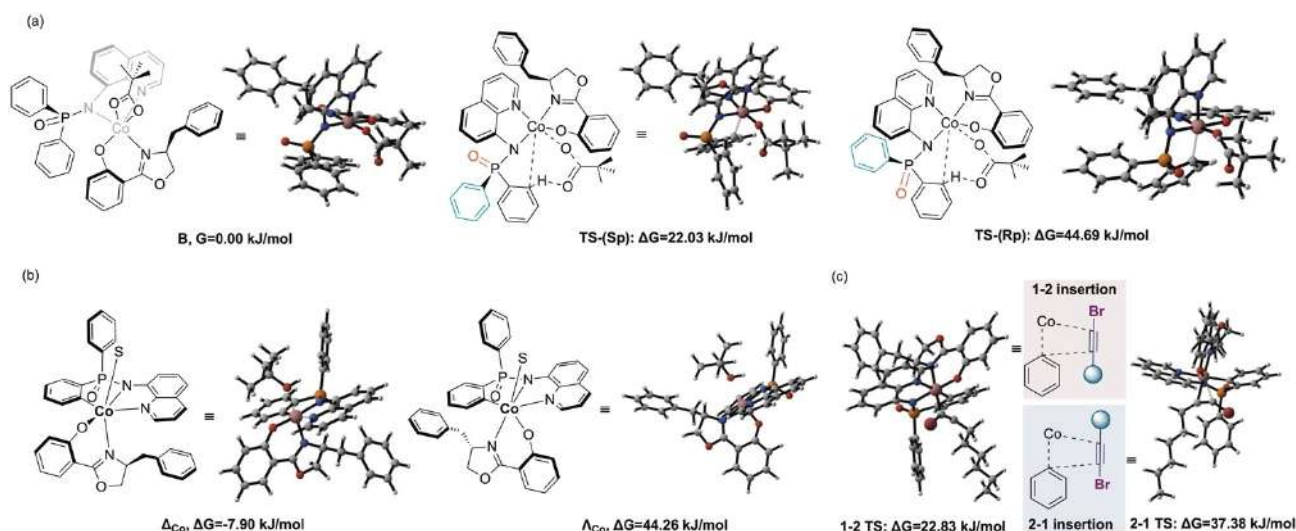
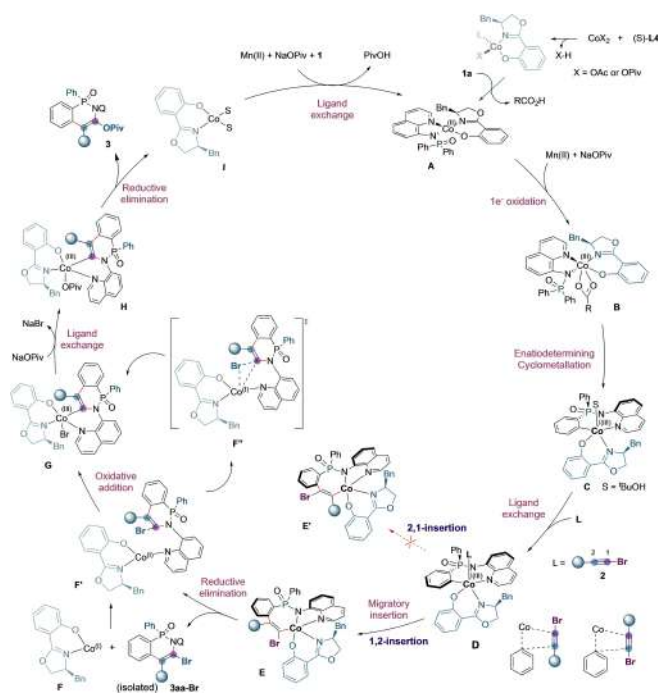


Figure 1. DFT calculations on (a) enantioselective C–H activation, (b) optimized structures for *mer*-(*Sc*,*Sp*)-[Δ_{Co-1}] and *mer*-(*Sc*,*Sp*)-[Λ_{Co-1}] and (c) migratory insertions step.

as a catalyst, furnishing the desired product **3aa** with 12 % yield and 99 % *ee* (Scheme 4c). The low yield of product **3aa** might be due to the presence of strongly coordinating DMAP ligand. These results collectively suggest the octahedral complex *mer*-(*Sc*,*Sp*)-[**A**_{C_{o-1a}] possibly take part in the desymmetrization process and the C–H activation likely enantiodetermining step. Stoichiometric reaction between isolated cobalt complex *mer*-(*Sc*,*Sp*)-[**A**_{C_{o-1a}] and bromoalkyne **2a** in the absence of NaOPiv in *tert*-butanol provided vinyl bromide **3aa-Br** instead of **3aa** suggesting that the reaction proceeds through annulation pathway before exchange carboxylate to deliver the desired product **3aa-Br** (Scheme 4d). To understand whether the Br- to OPiv conversion is mediated by metal or not, we performed the reaction with **3aa-Br** under standard conditions or treated solely with sodium pivalate without cobalt in *tert*-BuOH at 60 °C for 24 hours (Scheme 4e). As expected, the bromo functionality remains intact in **3aa-Br** in both experiments (Scheme 4e (i)). In contrast, the bromo compound converted to the corresponding the bromo compound converted to the corresponding product **3aa** when it was subjected to a catalytic reaction of **1d** with 1-bromonon-1-yne **2a**, providing both **3da** and **3aa** in 79 % and 31 % isolated yields (Scheme 4e (ii)), suggesting that the in situ-generated low-valent cobalt(I) species undergo oxidative addition with **3aa-Br** followed by ligand exchange with pivalic acid and reductive elimination furnish the expected products **3aa** and **3da**.}}

We then demonstrate the possible derivatization of **3aa** using reported nickel-catalyzed enantiospecific cross-coupling reaction via C–O bond activation (unoptimized) with the retention of 97 % *ee* of **3aa-Ph** (Scheme 4(f)).^[20]

Based on the control experiments, DFT studies and literature precedents,^[13,14,21–22] we propose a plausible mechanism as shown in Scheme 5. The cobalt(II) acetate undergoes sequential ligand exchange with Salox (**S**)-**L4** and phosphinamides **1a** led to Co(II) intermediate **A**. There-



Scheme 5. Plausible catalytic cycle.

after, manganese (II) promotes facile oxidation of Co(II) complex under air in the presence of sodium pivalate to the corresponding Co(III) pivalate octahedral intermediate **B**, and subsequent enantio-determining carboxylate-assisted C–H cleavage provide diastereoselective cobaltacycle **C** (*mer*-(*Sc,Sp*)-[Δ_{Co-1}]). Coordination of bromoalkyne **2** and subsequent regioselective 1,2-insertion between Co–C bond results in the seven-membered metallacycle **E** which is energetically preferred pathway than the 2,1-insertion pathway. Reductive elimination of intermediate **E** liberates vinylbromo intermediate **3aa-Br** and Co(I) species **F**.

Alternatively, it can undergo direct **F'** to **G** (via **F''**) conversion without liberating **3aa-Br**. The proximity of vinyl bromide may readily proceed for oxidative addition with electron rich cobalt(I) to intermediate **G**, and subsequent ligand exchange with carboxylate followed by reductive elimination to provide Co(I) intermediate **I**. The liberation of product **3aa** and subsequent coordination of **1a** in the presence of carboxylate ligand and Mn regenerate the active Co(II) intermediate **A** for the next catalytic cycle.

Conclusion

In conclusion, we developed an efficient protocol for an unprecedented asymmetric C–H annulation with inverse regioselectivity using haloalkynes catalyzed by cobalt-Salox system to access a new class of chiral phosphorus compounds with excellent enantiopurity. The reaction scope is very general and high *ee*'s were obtained with most of the isolated products. The experimental studies including isolation of cobaltacycle (*X*-ray) and their usage in catalytic as well as stoichiometric study further confirm the involvement of octahedral cobaltacycle. Further, DFT calculations suggest that (*mer*-(*Sc,Sp*)-[Δ_{Co-1}]) is the major diastereomer among the other possible diastereomers, and 1,2-insertion of bromoalkyne is favoured over 2,1-insertion pathway. The overall catalytic cycle proceeds through Co(II)–Co(III)–Co(I) catalytic pathways for the annulation process and Co(I)–Co(III)–Co(I) pathway for the oxygenation step.

Acknowledgements

Financial support provided by SERB (CRG/2020/001282) to support this research work is gratefully acknowledged. A. D., R. M., H. S. R. & S. K. acknowledges CSIR and IITK for their fellowship.

Conflict of Interest

The authors declare no conflict of interest.

Data Availability Statement

The data that support the findings of this study are available in the supplementary material of this article.

Keywords: Asymmetric Catalysis • C–H Bond Functionalization • Cobalt • Regioselectivity • Salox

- [1] a) K. N. Houk, B. List, *Acc. Chem. Res.* **2004**, *37*, 487–487; b) J. S. Carey, D. Laffan, C. Thomson, M. T. Williams, *Org. Biomol. Chem.* **2006**, *4*, 2337–2347; c) S. Mayer, B. List, *Angew. Chem. Int. Ed.* **2006**, *45*, 4193–4195; d) S. Mukherjee, J. W. Yang, S. Hoffmann, B. List, *Chem. Rev.* **2007**, *107*, 5471–5569;

- e) Y. Park, S. Chang, *Nat. Catal.* **2019**, *2*, 219–227; f) S. Aubert, T. Katsina, S. Arseniyadis, *Org. Lett.* **2019**, *21*, 2231–2235; g) J. E. Gillespie, A. Fanourakis, R. J. Phipps, *J. Am. Chem. Soc.* **2022**, *144*, 18195–18211; h) C. Bolm, J. A. Gladysz, *Chem. Rev.* **2003**, *103*, 2761–2762.
- [2] a) H. Jiang, X. Zhao, W. Zhang, Y. Liu, H. Li, Y. Cui, *Angew. Chem. Int. Ed.* **2023**, *62*, e202214748; b) W. Zhao, H.-X. Lu, W.-W. Zhang, B.-J. Li, *Acc. Chem. Res.* **2023**, *56*, 308–321; c) J. Zhou, D. Wang, W. Xu, Z. Hu, T. XU, *J. Am. Chem. Soc.* **2023**, *145*, 2081–2087; d) J. M. Ovian, P. Vojáčeková, E. N. Jacobsen, *Nature* **2023**, <https://doi.org/10.1038/s41586-023-05804-3>; e) A. F. Zahrt, S. V. Athavale, S. E. Denmark, *Chem. Rev.* **2020**, *120*, 1620–1689; f) T. Yu, Z. Ding, W. Nie, J. Jiao, H. Zhang, Q. Zhang, C. Xue, X. Duan, Y. M. A. Yamada, P. Li, *Chem. Eur. J.* **2020**, *26*, 5729–5747; g) C. Prentice, J. Morrisson, A. D. Smith, E. Zysman-Colman, *Beilstein J. Org. Chem.* **2020**, *16*, 2363–2441; h) T. B. Wright, P. A. Evans, *Chem. Rev.* **2021**, *121*, 9196–9242.
- [3] a) B. Zhan, L. Jin, B.-F. Shi, *Trends Chem.* **2022**, *4*, 220–235; b) Q. Zhang, L.-S. Wu, B.-F. Shi, *Chem* **2022**, *8*, 384–413; c) S. K. Sinha, G. Zanoni, D. Maiti, *Asian J. Org. Chem.* **2018**, *7*, 1178–1192; d) A. Das, N. T. Patil, *Chem. Eur. J.* **2022**, *28*, e20210437; e) B. Zu, Y. Guo, J. Ke, C. He, *Synthesis* **2021**, *53*, 2029–2042; f) Q. Gu, Z.-J. Wu, S.-L. You, *Bull. Chem. Soc. Jpn.* **2021**, *94*, 641–647; g) C.-X. Liu, Q. Gu, S.-L. You, *Trends Chem.* **2020**, *2*, 737–749.
- [4] a) Z. Zhuang, J.-Q. Yu, *J. Am. Chem. Soc.* **2020**, *142*, 12015–12019; b) E. L. Lucas, N. Y. S. Lam, Z. Zhuang, H. S. S. Chan, D. A. Strassfeld, J.-Q. Yu, *Acc. Chem. Res.* **2022**, *55*, 537–550; c) D. E. Hill, J.-Q. Yu, D. G. Blackmond, *J. Org. Chem.* **2020**, *85*, 13674–13679; d) L. Hu, P.-X. Shen, Q. Shao, K. Hong, J. X. Qiao, J.-Q. Yu, *Angew. Chem. Int. Ed.* **2019**, *58*, 2134; e) G. Li, J. Jiang, H. Xie, J. Wang, *Chem. Eur. J.* **2019**, *25*, 4688–4694; f) C.-X. Liu, W.-W. Zhang, S.-Y. Yin, Q. Gu, S.-L. You, *J. Am. Chem. Soc.* **2021**, *143*, 14025–14040; g) Pan, S.-Y. Yin, S.-B. Wang, Q. Gu, S.-L. You, *Angew. Chem. Int. Ed.* **2021**, *60*, 15510; h) Ł. Woźniak, J.-F. Tan, Q.-H. Nguyen, A. Madron du Vigné, V. Smal, Y.-X. Cao, N. Cramer, *Chem. Rev.* **2020**, *120*, 10516–10543; i) T. Yoshino, S. Matsunaga, *ACS Catal.* **2021**, *11*, 6455–6466; j) X. Yang, G. Zheng, X. Li, *Angew. Chem.* **2019**, *131*, 328–332; k) H. Wang, Y. Park, Z. Bai, S. Chang, G. He, G. Chen, *J. Am. Chem. Soc.* **2019**, *141*, 7194–7201; l) Y. Kato, L. Lin, M. Kojima, T. Yoshino, S. Matsunaga, *ACS Catal.* **2021**, *11*, 4271–4277; m) S. Satake, T. Kurihara, K. Nishikawa, T. Mochizuki, M. Hatano, K. Ishihara, T. Yoshino, S. Matsunaga, *Nat. Catal.* **2018**, *1*, 585–591; n) L.-T. Huang, Y. Hirata, Y. Kato, L. Lin, M. Kojima, T. Yoshino, S. Matsunaga, *Synthesis* **2022**, *54*, 4703–4710.
- [5] a) L. Wozniak, N. Cramer, *Trends Chem.* **2019**, *1*, 471–478; b) J. Loup, U. Dhawa, F. Pesciaoli, J. Wencel-Delord, L. Ackermann, *Angew. Chem. Int. Ed.* **2019**, *58*, 12803–12818; c) N. Kaplaneris, L. Ackermann, *Beilstein J. Org. Chem.* **2022**, *18*, 86–88; d) R. Mandal, B. Garai, B. Sundararaju, *ACS Catal.* **2022**, *12*, 3452–3506; e) P. Gandeepan, T. Müller, D. Zell, G. Cera, S. Warratz, L. Ackermann, *Chem. Rev.* **2019**, *119*, 2192–2452; f) T. Yoshino, *Bull. Chem. Soc. Jpn.* **2022**, *95*, 1280–1288; g) T. Yoshino, S. Matsunaga, *Synlett* **2019**, *30*, 1384–1400.
- [6] a) T. Yoshino, S. Matsunaga, *Adv. Synth. Catal.* **2017**, *359*, 1245–1262; b) Y. Komagalla, N. Chatani, *Coord. Chem. Rev.* **2017**, *350*, 117–135; c) L. Lukasevics, A. Cizikovs, L. Grigorjeva, *Chem. Commun.* **2021**, *57*, 10827–10841; d) A. Baccalini, S. Vergura, P. Dolui, G. Zanoni, D. Maiti, *Org. Biomol. Chem.* **2019**, *17*, 10119–10141; e) N. Rajesh, N. Barsu, B. Sundararaju, *Tetrahedron Lett.* **2019**, *59*, 862–868.
- [7] a) K. Ozols, Y.-S. Jang, N. Cramer, *J. Am. Chem. Soc.* **2019**, *141*, 5675–5680; b) A. G. Herranz, N. Cramer, *ACS Catal.* **2021**, *11*, 11938; c) K. Ozols, S. Onodera, L. Wozniak, N. Cramer,

- Angew. Chem. Int. Ed.* **2021**, *60*, 655–659; Also see: d) Y. Zheng, W.-Y. Zhang, Q. Gu, C. Zheng, S.-L. You, *Nat. Commun.* **2023**, *14*, 1094.
- [8] a) F. Pesciaoli, U. Dhawa, J. C. A. Oliveira, R. Yin, M. John, L. Ackermann, *Angew. Chem. Int. Ed.* **2018**, *57*, 15425–15429; b) Z.-J. Zhang, S.-W. L. J. C. A. Oliveira, Y. Li, X. Chen, S.-Q. Zhang, L.-C. Xu, T. Rogge, X. Hong, L. Ackermann, *Nat. Commun.* **2023**, *14*, 3149.
- [9] a) Y. Hirata, D. Sekine, Y. Kato, L. Lin, M. Kojima, T. Yoshino, S. Matsunaga, *Angew. Chem. Int. Ed.* **2022**, *61*, e202205341; b) T. Kurihara, M. Kojima, T. Yoshino, S. Matsunaga, *Asian J. Org. Chem.* **2020**, *9*, 368–371; c) S. Fukagawa, Y. Kato, R. Tanaka, M. Kojima, T. Yoshino, S. Matsunaga, *Angew. Chem. Int. Ed.* **2019**, *58*, 1153–1157.
- [10] Y.-B. Zhou, T. Zhou, P.-F. Qian, J.-Y. Li, B.-F. Shi, *ACS Catal.* **2022**, *12*, 9806–9811.
- [11] a) L. Grigorjeva, O. Daugulis, *Angew. Chem. Int. Ed.* **2014**, *53*, 10209–10212; b) S. Rej, Y. Ano, N. Chatani, *Chem. Rev.* **2020**, *120*, 1788–1887.
- [12] a) S. Maity, R. Kancherla, U. Dhawa, E. Hoque, S. Pimparkar, D. Maiti, *ACS Catal.* **2016**, *6*, 5493–5499; b) D. Kalsi, N. Barsu, B. Sundararaju, *Chem. Eur. J.* **2018**, *24*, 2360–2364.
- [13] a) B.-J. Wang, G.-X. Xu, Z.-W. Huang, X. Wu, X. Hong, Q.-J. Yao, B.-F. Shi, *Angew. Chem. Int. Ed.* **2022**, *61*, e202208912; b) X.-J. Si, D. Yang, M.-C. Sun, D. Wei, M.-P. Song, J.-L. Niu, *Nat. Synth.* **2022**, *1*, 709–718; c) Q.-J. Yao, J.-H. Chen, H. Song, F.-R. Huang, B.-F. Shi, *Angew. Chem. Int. Ed.* **2022**, *61*, e202202892; d) J.-H. Chen, M.-Y. Teng, F.-R. Huang, H. Song, Z.-K. Wang, H.-L. Zhuang, Y.-J. Wu, X. Wu, Q.-J. Yao, B.-F. Shi, *Angew. Chem. Int. Ed.* **2022**, *61*, e202210106; e) T. Li, L. Shi, X. Wang, C. Yang, D. Yang, M.-P. Song, J.-L. Niu, *Nat. Commun.* **2023**, *14*, 5271; f) Z.-K. Wang, Y.-J. Wu, Q.-J. Yao, B.-F. Shi, *Angew. Chem. Int. Ed.* **2023**, *62*, e202304706; g) Y.-J. Wu, Z.-K. Wang, Z.-S. Jai, J.-H. Chen, F.-R. Huang, B.-B. Zhan, Q.-J. Yao, B.-F. Shi, *Angew. Chem. Int. Ed.* **2023**, *62*, e202310004; h) Y.-J. Wu, J.-H. Chen, M.-Y. Teng, X. Li, T.-Y. Jaing, F.-R. Huang, Q.-J. Yao, B.-F. Shi, *J. Am. Chem. Soc.* **2023**, *145*, 24499–24505; i) X. Wang, X.-J. Si, Y. Sun, Z. Wei, M. Xu, D. Yang, L. Shi, M.-P. Song, J.-L. Niu, *Org. Lett.* **2023**, *25*, 6240–6245.
- [14] a) T. von Münchow, S. Dana, Y. Xu, B. Yuan, L. Ackermann, *Science* **2023**, *379*, 1036–1042; b) D. Yang, X. Zhang, X. Wang, X.-J. Si, J. Wang, D. Wei, M.-P. Song, J.-L. Niu, *ACS Catal.* **2023**, *13*, 4250–4260; c) Q.-J. Yao, F.-R. Huang, J.-H. Chen, M.-Y. Zhong, B.-F. Shi, *Angew. Chem. Int. Ed.* **2023**, *62*, e202218533; d) X.-J. Si, X. Zhao, J. Wang, X. Wang, Y. Zhang, D. Yang, M.-P. Song, J.-L. Niu, *Chem. Sci.* **2023**, <https://doi.org/10.1039/D3SC01787G>; also, see: e) T. Liu, W. Zhang, C. Xu, Z. Xu, D. Song, W. Qian, G. Lu, C.-J. Zhang, W. Zhong, F. Ling, *Green Chem.* **2023**, *25*, 3606–3614; f) Y. Lin, T. von Münchow, L. Ackermann, *ACS Catal.* **2023**, *14*, 9713–9723; g) T. Li, L. Shi, X. Wang, C. Yang, D. Yang, M.-P. Song, J.-L. Niu, *Nat. Commun.* **2023**, *14*, 5271; h) G. Zhou, J.-H. Chen, Q.-J. Yao, F.-R. Huang, Z.-K. Wang, B.-F. Shi, *Angew. Chem. Int. Ed.* **2023**, *62*, e202302964; i) T. Li, L. Shi, X. Zhao, X. Zhao, J. Wang, X.-J. Si, D. Yang, M.-P. Song, J.-L. Niu, *Org. Lett.* **2023**, *25*, 5191–5196.
- [15] a) T. Piou, F. Romanov-Michailidis, M. Romanova-Michaelides, K. E. Jackson, N. Semakul, T. D. Taggart, B. S. Newell, C. D. Rithner, R. S. Paton, T. Rovis, *J. Am. Chem. Soc.* **2017**, *139*, 1296–1310; b) T. Piou, F. Romanov-Michailidis, M. A. Ashley, M. Romanova-Michaelides, T. Rovis, *J. Am. Chem. Soc.* **2018**, *140*, 9587–9593; c) T. Piou, T. Rovis, *Acc. Chem. Res.* **2018**, *51*, 170–180; d) E. A. Trifonova, N. M. Ankudinov, M. V. Kozlov, M. Y. Sharipov, Y. V. Nelyubina, D. S. Perekalin, *Chem. Eur. J.* **2018**, *24*, 16570–16575.
- [16] a) B. Garai, M. R. Ali, R. Mandal, B. Sundararaju, *Org. Lett.* **2023**, *25*, 2018–2023; b) B. Khan, V. Dwivedi, B. Sundararaju, *Adv. Synth. Catal.* **2020**, *362*, 1195–1200; c) P. Chakraborty, N. Garg, E. Manoury, R. Poli, B. Sundararaju, *ACS Catal.* **2020**, *10*, 8023–8031; d) D. Kalsi, S. Dutta, N. Barsu, M. Rueping, B. Sundararaju, *ACS Catal.* **2018**, *8*, 8115–8120; e) R. Mandal, B. Emayavaramban, B. Sundararaju, *Org. Lett.* **2018**, *20*, 2835–2838; f) R. Mandal, B. Sundararaju, *Org. Lett.* **2017**, *19*, 2544–2547; g) M. Sen, B. Emayavaramban, N. Barsu, J. R. Premkumar, B. Sundararaju, *ACS Catal.* **2016**, *6*, 2792–2796; h) N. Barsu, S. K. Bolli, B. Sundararaju, *Chem. Sci.* **2017**, *8*, 2431–2435.
- [17] L. Gong, S. P. Mulcahy, D. Devarajan, K. Harms, G. Frenking, E. Meggers, *Inorg. Chem.* **2010**, *49*, 7692–7699.
- [18] See the Supporting Information for more details.
- [19] Deposition numbers 2298731 (**3an**), 2298732 (**3da**) and 2298308 (*mer*-(*Sc,Sp*)-[Δ_{Co-III}]) contain the supplementary crystallographic data for this paper. These data are provided free of charge by the joint Cambridge Crystallographic Data Centre and Fachinformationszentrum Karlsruhe Access Structures service.
- [20] Q. Zhou, H. D. Srinivas, S. Dasgupta, M. P. Watson, *J. Am. Chem. Soc.* **2013**, *135*, 3307–3310.
- [21] a) L. D. Caspers, B. J. Nachtsheim, *Chem. Asian J.* **2018**, *13*, 1231; b) N. Sauermaier, M. J. Gonzalez, L. Ackermann, *Org. Lett.* **2015**, *17*, 5316–5319; c) V. G. Landge, S. P. Midya, J. Rana, D. R. Shinde, E. Balaraman, *Org. Lett.* **2016**, *18*, 5252–5255; d) V. G. Landge, G. Jaiswal, E. Balaraman, *Org. Lett.* **2016**, *18*, 812–815; e) E. Tan, A. I. Konovalov, G. A. Fernandez, R. Dorel, A. M. Echavarren, *Org. Lett.* **2017**, *19*, 5561–5564.
- [22] a) T. T. Nguyen, L. Grigorjeva, O. Daugulis, *ACS Catal.* **2016**, *6*, 551–554; b) D. Kalsi, B. Sundararaju, *Org. Lett.* **2015**, *17*, 6118–6121; c) O. Planas, C. J. Whiteoak, A. Company, X. Ribas, *Adv. Synth. Catal.* **2015**, *357*, 4003–4012; d) R. Manoharana, M. Jeganmohan, *Org. Biomol. Chem.* **2018**, *16*, 8384–8389; e) R. Mei, H. Wang, S. Warratz, S. A. Macgregor, L. Ackermann, *Chem. Eur. J.* **2016**, *22*, 6759–6763; f) X.-C. Li, C. Du, H. Zhang, J.-L. Niu, M.-P. Song, *Org. Lett.* **2019**, *21*, 2863–2866; g) C. Kuai, L. Wang, B. Li, Z. Yang, X. Cui, *Org. Lett.* **2017**, *19*, 2102–2105; h) J. Bora, M. Dutta, B. Chetia, *Tetrahedron* **2023**, *132*, 133248; i) R. Mandal, B. Garai, B. Sundararaju, *J. Org. Chem.* **2021**, *86*, 9407–9417; j) R. Mandal, N. Barsu, B. Garai, A. Das, D. Perekalin, B. Sundararaju, *Chem. Commun.* **2021**, *57*, 12167–12170; k) H. Huang, S. Nakanowatari, L. Ackermann, *Org. Lett.* **2017**, *19*, 4620–4623.

Manuscript received: October 6, 2023

Accepted manuscript online: December 14, 2023

Version of record online: December 28, 2023